The range of Jupiter's flow structures fitting the Juno asymmetric gravity measurements

Keren Duer[1], **Eli Galanti**[1] **and Yohai Kaspi**[1]

[1]Department of Earth and Planetary Sciences, Weizmann Institute of Science, Rehovot, Israel

Key Points:

- Jupiter's asymmetric gravity field confines the vertical profile of the flow, with each harmonic constraining the flow at a different depth
- Deep zonal flows with a meridional profile significantly different from that of the cloud-level are possible, but statistically unlikely.
- A smoother flow profile at depth, as implied by the Juno microwave measurements, is consistent with the gravity measurements.

Corresponding author: Keren Duer, `keren.duer@weizmann.ac.il`

Abstract

The asymmetric gravity field measured by the Juno spacecraft allowed estimation of the depth of Jupiter's zonal jets, showing that the winds extend approximately 3000 km beneath the cloud-level. This estimate was based on an analysis using a combination of all four measured odd gravity harmonics, so that the wind profile dependence on each of them separately has not been investigated. Furthermore, these calculations assumed the meridional profile of the cloud-level wind extends to depth. However, it is possible that the interior jet profile varies from that of the cloud-level as hinted by the Juno microwave measurement that finds a smoother nadir brightness temperature profile at depth compared to the cloud-level. Here we analyze in detail the possible meridional and vertical structure of Jupiter's deep jet-streams. We find that each odd gravity harmonic constrains the flow at a different depth, with J_3 being the most dominant at depths below 3000 km, J_5 being the most restrictive overall and J_9 not constraining the flow at all if the other odd harmonics are within the measurement range. Interior flow profiles constructed from perturbations to the cloud-level winds allow a more extensive range of vertical wind profiles, yet when the profiles differ substantially from the cloud-level the ability to match the gravity data reduces significantly. Overall, we find that while interior wind profiles which differ substantially from those at the cloud-level are possible, they are statistically unlikely. However, slightly smoother profiles, which match the MWR profile at depth are still compatible with the gravity measurements.

Plain Language Summary

Jupiter's North-South asymmetric gravity field that was measured by the Juno spacecraft, currently orbiting Jupiter, allowed estimating the depth of the jet-streams (associated with the famous visible bands) to approximately 3000 km. This estimate was based on using all the gravity field (harmonics) combined, however there is also information about the structure of the flow hidden in each of the gravity harmonics alone. Here we analyze those measurements and show how each of them constrains the flow at a different depth We also analyze systematically the statistical likelihood of wind profiles that differ from that observed at the cloud-level with various wind profiles at depth. We find that for Jupiter's measured cloud-level jet streams, only a relatively narrow envelope of vertical structures allow fitting the gravity data. Although other jet profiles that are different than the observed at the cloud-level are feasible (still consistent with the gravity data), they are statistically unlikely. The Juno microwave radiometer instrument suggests that the wind profile at depth varies from that of the cloud-level, with the winds having a smoother silhouette. We find that such profile can still match the gravity data as long as the variation from the cloud-level wind is not substantial.

1 Introduction

The Juno spacecraft has provided an unprecedented glance into Jupiter's atmospheric flows below the cloud-level. The high precision gravity measurements, particularly the odd gravitational harmonics repeated in multiple passes (Iess et al., 2018), presented an opportunity to estimate the depth and structure of Jupiter's zonal jets. It was found that the zonal jets are deep and penetrate to approximately 3000 km below the cloud-level (Kaspi et al., 2018). Below this depth, the even gravitational harmonics indicate that Jupiter is rotating nearly as a solid body (Guillot et al., 2018). However, the details of the decay in the flow strength with depth have yet to be determined. There appear to be remnants of the jets even below 4000 km, and since at this depth the electrical conductivity in Jupiter is relatively high (Liu et al., 2008; French et al., 2012), there might be interaction between the flow and the magnetic field (Cao & Stevenson, 2017; Galanti, Cao, & Kaspi, 2017; Duer et al., 2019; Moore et al., 2019). Understanding the gravity

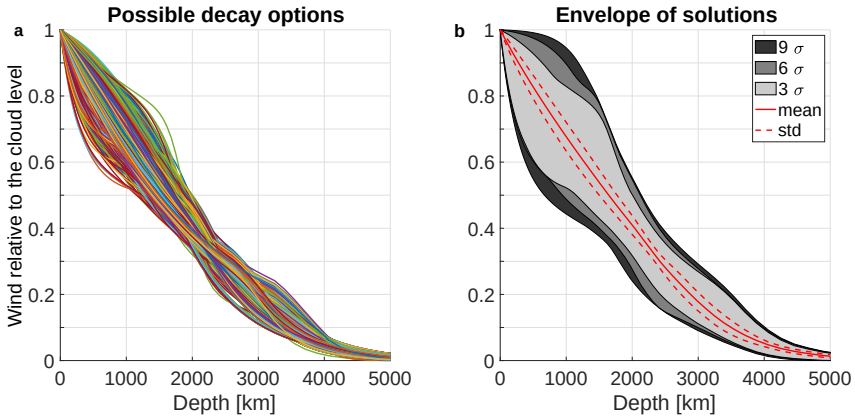

Figure 1. (a) Examples of decay options that fit all four measured odd gravity harmonics (J_n) within the 3σ sensitivity range of Juno and using Jupiter's exact observed cloud-level flows (Tollefson et al., 2017). The ordinate represents the fraction of the wind velocity relative to the wind at the cloud-level. (b) Envelope of all possible solutions (light gray), the average solution of all options (red line), their standard deviation (dashed red lines) and envelope of solutions satisfying larger range (darker gray with rising uncertainty range).

harmonic signature and the flow structure below the cloud level is with high importance in order to complete the picture.

The even gravity harmonics are used to constrain the internal density structures of gas giants (e.g. Hubbard et al., 1974; Hubbard et al., 1975; Helled et al., 2010; Nettelmann et al., 2013). The higher order (even) gravity harmonics are sensitive to the outer regions of the planet (Zharkov & Trubitsyn, 1974; Guillot & Gautier, 2007; Nettelmann et al., 2013). Their exact value is defined by the density distribution throughout the planet and the planet's rotation, composition, shape, mass, and radius. Since for a static gas planet, the odd harmonics are identically zero, any gravitational asymmetry between north and south would indicate on a dynamical source generating those asymmetries (Kaspi, 2013). The depth sensitivity of each of the odd gravity harmonics separately has yet to be examined.

Juno measured with high precision the gravity harmonics up to J_{10}, including significant odd values. The measured values and error range are: $J_3\left(\times 10^{-8}\right) = -4.24 \pm 0.91$, $J_5\left(\times 10^{-8}\right) = -6.89 \pm 0.81$, $J_7\left(\times 10^{-8}\right) = 12.39 \pm 1.68$ and $J_9\left(\times 10^{-8}\right) = -10.58 \pm 4.35$ (Iess et al., 2018). The relation between the density anomaly to the flow (thermal wind balance) allows constraining the deep flow structure within the planet (Kaspi et al., 2010; Kaspi, 2013; Kaspi et al., 2018). Assuming that the cloud level zonal wind structure is extended towards Jupiter's interior using a scaling factor, one can find many solutions for the deep flow structure that satisfy all four odd gravity harmonics within the uncertainty range. Yet, all those solutions are within a relatively narrow envelope of solutions (Fig. 1). For a full description of the figure and the search for possible solutions see subsections 2.1 and 2.2.

However, the meridional structure of the zonal wind is not necessarily constant with depth. The cloud-level wind itself has a measurement error (Garcıa-Melendo & Sánchez-Lavega, 2001; Salyk et al., 2006; Tollefson et al., 2017), and as it extends inward the profile might vary, although any such variation must be accompanied with a meridional temperature gradient as well. Some evidence to such meridional variations come from the Juno microwave radiometer (MWR) measurements showing that nadir brightness temperature profile (dominated by the ammonia abundance), becomes smoother with depth

(Bolton et al., 2017; Li et al., 2017; Ingersoll et al., 2017). Although this measurement is not necessarily correlated with temperature, it does coincide somewhat with the zonal wind profile at the cloud-level (Bolton et al., 2017), and thus might provide a hint to the vertical variation of the zonal wind profile in the upper 300 km. In this study we investigate if zonal wind profiles that have a smoother meridional variation (resembling the MWR measurements) can be consistent with the gravity measurements.

Previous work on constraining the deep flow structure was done using all four measured gravity harmonics combined (e.g. Kaspi et al., 2018; Kong et al., 2018). However, an important question is how each gravity harmonic individually constrains the flow strength at different depths. Here, we examine the individual contribution of each odd gravity harmonic, with emphasis on the depth of influence and the relation to the cloud-level zonal wind profile.

In order to provide a systematic analysis we take a hierarchal approach where we increase the level of complexity of the variation of the wind structure, and in all cases explore what is the range of solutions that match the gravity measurements. We begin with solutions which are identical to the cloud-level profile and allow only for the vertical decay to vary. Then, we relax the meridional profile of the zonal wind and allow variations to the measured cloud-level profile along with the varying vertical decay. Finally, we examine random meridional profiles that are not related at all to Jupiter's measured cloud-level profile, exploring the possibility that the interior wind structure, which is influencing the gravity measurements, is completely different than the cloud-level flow. Following this logic, we also search for solutions with smoother wind profiles at depth, resembling the MWR measurements at 300 km (channel 1), and calculate the vertical structure of such flows that can match also the gravity data.

The paper is structured as follows: in section 2 we introduce the theoretical background for this analysis, connecting the gravity measurements and the wind profile. In section 3 we present the possible solutions for Jupiter's wind structure while excluding a specific harmonic, and discuss the ability to find solutions for the anomalous gravity field of different meridional arrangements and depth dependent meridional structures. Finally, in section 4 we discuss the significance and conclusions of this study.

2 Methodology

To understand the depth sensitivity and relation to the latitudinal structure of each odd gravity harmonic, we introduce here the general equations relating deep flow structures to the odd harmonics, the possible vertical decay structures and latitudinal structures used in this study.

2.1 Relation between the flow structure and the gravity anomaly

The density distribution within Jupiter can be described by the zonal gravity harmonics (J_n), which describe the external gravitational field of the planet in equilibrium (Zharkov & Trubitsyn, 1974). The gravity multipole harmonics can be represented by

$$J_n = -\frac{1}{MR_J^n}\int \rho r^n P_n d^3 r, \tag{1}$$

where M and R_J are Jupiter's mass and equatorial radius, respectively, n is the harmonic degree, ρ is density, r is the radial coordinate and P_n is the n-th Legendre polynomial (Hubbard, 1984). The density can be decomposed such that $\rho(r,\theta) = \widetilde{\rho}(r,\theta) + \rho'(r,\theta)$, where $\widetilde{\rho}(r,\theta)$ is the static component that is determined mostly by the planet's shape and rotation (Hubbard, 2012), and $\rho'(r,\theta)$ is the dynamical anomaly representing fluid velocities that alter from solid body rotation with θ being latitude (Kaspi et al., 2010). The zonal gravity harmonics that represent only the dynamical part of the flow (ΔJ_n)

can be calculated by integrating the density anomaly and its projection onto the Legendre polynomials in spherical coordinates such that

$$\Delta J_n = -\frac{2\pi}{MR_J^n}\int_0^{R_J}\int_{-1}^{1}\rho'\left(r,\mu\right)r^{n+2}P_n\left(\mu\right)d\mu dr, \tag{2}$$

where $n = 2, ..., N$ are the harmonic degrees and $\mu = r\sin\left(\theta\right)$. Since an oblate planet with no dynamics is symmetric between north and south, the density anomaly represented by the odd harmonics ($n = 3, 5, ..$) should be identically zero if the flow pattern is symmetric or if the dynamics are shallow. However, Juno measured four odd gravity harmonics, indicating a strong asymmetric pattern exists in Jupiter's flow field (Iess et al., 2018).

The rapid rotation and size of the planet (small Rossby number) imply that this asymmetry can be directly related to zonal flows, since to first order, the leading balance in Jupiter is a balance between the flow related Coriolis forces and the thermodynamic anomaly (Kaspi et al., 2010, 2016, 2018). This balance is known as thermal wind balance (Pedlosky, 1987; Kaspi et al., 2009). If only zonal flows are considered, thermal wind balance can be written as

$$2\Omega\frac{\partial}{\partial z}\left(\tilde{\rho}u\right) = g_0\frac{\partial}{\partial\theta}\rho', \tag{3}$$

where Ω is Jupiter's rotation rate, u is the zonal flow, g_0 is the mean gravitational acceleration and z is the direction parallel to the rotation axis. Galanti, Kaspi, and Tziperman (2017) showed that a higher order expansion, beyond thermal wind, provides only a small (less than 10%) correction for determining the deep flow dynamics, and therefore for the purpose of studying the overall vertical structure we can neglect it.

We search for possible deep wind structures that can explain each one of the measured odd gravity harmonics (J_3, J_5, J_7, and J_9). Unlike previous studies (e.g. Kaspi et al., 2018), we are not searching for an optimal solution with respect to the full error covariance matrix. Any vertical wind structure that fits the odd measured gravity harmonics within the uncertainty range of Juno is considered a possible solution for the flow. This allows to examine the full range of possible solutions, without converging to a single decay structure of the flow. For example, the solution suggested by Kaspi et al. (2018) that considered the covariance matrix is not a solution here since the value of J_3 is not within the measured error. We test the depth sensitivity of each harmonic by excluding it in the calculations, and examining the difference between the vertical profiles that include the specific J_n to those that do not.

2.2 Range of vertical decay structures

Taking an hierarchal approach with an increasing level of complexity, we first use the observed cloud-level wind as an upper boundary condition for the flow field, and assume the same profile continues inward. The possible deep flow structures are set to decay continuously from the cloud-level to few thousands of kilometers (Kaspi et al., 2018), using two decay regions and a maximum of two steps. The choice to divide the decay functions into two distinct regions rises from the possible magnetic field effects on the flow, expected at $r < 0.95\,R_J$ (Duer et al., 2019), which imply that once the electrical conductivity begins to be dominant the magnetic field acts to dissipate the flow (Liu et al., 2008; Gastine et al., 2014). Thus, for the lower part (the semi-conductive region), we chose an exponential decay (Eq. 6) that fits the exponential nature of the electrical conductivity within Jupiter (Nellis et al., 1992; Weir et al., 1996; French et al., 2012). For the upper part, the function includes both an exponent and hyperbolic tangent, which combined (Eq. 5) give a wide possible range of decay function.

The zonal flow vertical structure is defined therefore with six independent parameters chosen to cover an extensive range of vertical structures. The total zonal flow structure is

$$u(\theta, r) = u_{\rm top}(\theta, r) Q_s(r), \tag{4}$$

$$Q_s(r) = (1-\alpha)\exp\left(\frac{r-R_J}{H_1}\right) + \alpha\left[\frac{\tanh\left(-\frac{R_J-H_2-r}{\Delta H}\right)+1}{\tanh\left(\frac{H_2}{\Delta H}\right)+1}\right] \qquad R_T \le r \le R_J, \tag{5}$$

$$Q_s(r) = Q_s(r=R_T)\exp\left(\frac{r-R_T}{H_3}\right) \qquad r < R_T, \tag{6}$$

where $u_{\rm top}(r,\theta)$ is the wind at the cloud level, projected downwards in the direction parallel to the axis of rotation (Eq. 3), $Q_s(r)$ is the radial decay function (see examples in Fig. 1), representing the fraction of the cloud-level wind at every depth, and the set of parameters that forms the decay rate are bounded in the following limits: $0 \le \alpha \le 1$, $200 \le H_1 \le 2500$ km, $200 \le H_2 \le 2500$ km, $200 \le \Delta H \le 2500$ km, $0.95 \le R_T \le 0.975\,R_J$ and $100 \le H_3 \le 900$ km. The function Q_s is also smoothened at the transition depth. From each set of systematically random chosen parameters, we calculate the resulting density anomaly and the implied odd gravity harmonics, to find the depth sensitivity of each individual harmonic. This process is repeated 5×10^5 times to cover the full parameter space.

2.3 Varying the meridional profile of the cloud-level zonal wind

The assumption that Jupiter's zonal flow profile remains constant at all depths requires further investigation and cannot be taken as trivial. First, because the zonal wind profile is measured by tracking of cloud motions which itself has some uncertainty (Tollefson et al., 2017). Second, and most importantly, the assumption that the cloud-level profile extends perfectly to depth requires the flow to be barotropic which is not necessarily the case. On the other hand, any deviation from barotropic must be supported by horizontal temperature gradients, which themselves must be maintained by some internal mechanism (Showman & Kaspi, 2013). Internal convection models support the scenario that there may be internal shear over the upper few thousand kilometers, but the overall structure of the flow does not change much (Kaspi et al., 2009; Jones & Kuzanyan, 2009). Any significant deviation from the zonal wind structure observed as the cloud-level requires significant shear and correspondingly significant horizontal thermal gradients. As this is an open question, for the purpose of this analysis we examine several cases of meridional wind profiles, under the assumption that the wind structure possibly varies beneath the cloud-level. For the purpose of the gravity analysis this means that the new profile used occupies enough mass to affect the gravity field, and the cloud-level observed flow is limited to a shallow enough layer so it does not affect the gravity field.

The simplest case is clearly to use the measured profile at Jupiter's cloud level and allow its magnitude to decay with depth. A slightly less constraining option is to insert a perturbation to the measured profile, therefore keeping the general form and allow a varying level of modifications to the cloud-level flow. The perturbed winds chosen here are a good representation to the measured uncertainties in Jupiter's cloud-level wind (Garcia-Melendo et al., 2011; Tollefson et al., 2017), or to changes in the wind structure below the measured wind at the cloud-level as implied possibly by MWR. Finally, random meridional profiles of the zonal flow with a similar general spectra to Jupiter's are examined as well. For the three cases (measured meridional profile, perturbed meridional profiles and random meridional profiles), the zonal flow structure is chosen at the cloud level ($u_{\rm top}$, Eq. 4) and projected downward along the rotation axis with a range of vertical structures as described in subsection 2.2.

The modified Jupiter profiles are calculated by adding sine-like perturbations to the measured wind. The standard deviation for the perturbations in the modified profiles is $5\pm0.5\,\mathrm{ms}^{-1}$ (varies with latitudes), well within the measurement error (Garcia-Melendo et al., 2011; Tollefson et al., 2017). The perturbation is constructed as

$$\epsilon\left(\theta\right)=\sum_{n=1}^{10}\left[a_n\sin\left(2n\theta\right)+b_n\cos\left(2n\theta\right)\right], \tag{7}$$

where ϵ is the perturbation, a_n and b_n are random numbers that are normally distributed around zero with std of 2, and θ is latitude. We examine 1000 modified profiles, where each profile is being constructed by adding the perturbation to the measured wind. In addition, 1000 random profiles are constructed purely from the functions ϵ, but with a standard deviation of $30\,\mathrm{ms}^{-1}$. These profiles represent internal winds that are completely unrelated to the observed cloud-level winds.

2.4 Altering the meridional profile with depth according to MWR measurements

The nadir brightness temperature estimations from Juno's six-channel microwave radiometer (Bolton et al., 2017; Li et al., 2017) reveal a strong variation in latitude. The brightness temperature is related to the ammonia distribution (Ingersoll et al., 2017), and shows some resemblance to the zonal jet structure. At the cloud-level, the relation between the two is prominent (channel 6), while in the other channels it appears to fade-out as the MWR profiles become smoother. It is important to note that the MWR does not indicate the temperature (in which case the relation to the wind shear would be trivial through thermal wind balance), and therefore a direct correlation between the nadir brightness temperature and the zonal flows is not necessarily expected. However, since there is correlation in the upper levels, and to examine the possibility that the MWR measurements are correlated enough to temperature to indicate on the jets strength and profile beneath the cloud-level, we analyze a range of depth dependent meridional profiles, compatible with the nadir brightness temperature trends. For this analysis we consider a range of modified cases, where in each we set the wind strength in the six channels according to MWR results, and project the wind strength from channel 1 (~ 300 km) inwards as in previous cases (subsection 2.2). The wind at channel one is composed using a running average of N degrees, where $N=0,1,2,...,10$ (0 means that no running average is applied).

3 Results

3.1 Jupiter's cloud-level wind

The depth sensitivity of each odd measured gravity harmonic, according to Jupiter's measured zonal profile, is presented in Fig. 2. The gray envelope, the same envelope from Fig. 1b, is the boundary of all possible solutions that fit all four odd gravity harmonics within 3σ. Note that not all lines inside the gray envelope will necessarily generate a solution compatible with the measured gravity field. All additional solutions that are gained while excluding one of the odd gravity harmonics appears in Fig. 2 (cyan envelopes), and emphasizes the region that the *excluded* harmonic bounds the flow. The most insignificant influence is clearly of J_9 (Fig. 2d). It appears to add no solutions at all to the gray envelope, meaning, J_9 does not constrain the flow at any depth and in general if the other three odd values are still within Juno's 3σ. This is due to two factors: first, according to the equation for the gravity harmonics (Eq. 2), J_9 should be most sensitive to the outermost region (because of the $(r/R_J)^n$ dependence) where the density is minimal and might not indicate on the interior structure. Second, J_9 has the highest measurement error, and lowest signal to noise ratio (SNR), so even while fitting J_9, there is an extensive region of solutions, and excluding it does not add new solutions.

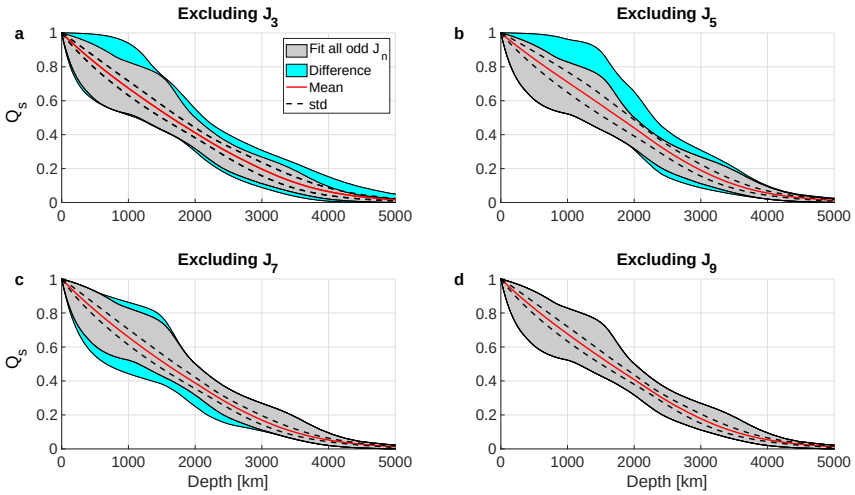

Figure 2. (a) The envelope of possible solutions that fit all four odd gravity harmonics (gray), the envelope of additional solutions once releasing J_3 (while still fitting J_5, J_7 and J_9) (cyan), the average of all decay options within the subplot (gray and cyan combined) (red), and the standard deviation of them (dashed black). The other panels are the same while excluding other J_n: (b) excluding J_5, (c) excluding J_7 and (d) excluding J_9. The results are a combination of 5×10^5 decay options. Note that the cyan color emphasizes the depth sensitivity of each gravity harmonic separately.

The largest influence on flow structure and depth sensitivity, comes from J_5 (Fig. 2b). It appears to set the upper boundary of the gray envelope from the cloud-level (0 km) to 3500 km, and a lower boundary of the gray envelope between 2000 to 3500 km. The strongest sensitivity is between the cloud-level and 3000 km. J_5 has the smallest measured 3σ value, and the smallest SNR, however its value is very similar to the SNR of J_7 thus the large influence of J_5 cannot be a result of its error alone. In a similar manner, J_3 is mostly sensitive between 3000 and 5000 km and between the cloud-level (0 km) to 1500 km (Fig. 2a). Note that for a flow structure that decays to zero velocities at 4000 km ($\sim 0.94\,R_J$) J_3 must be excluded. J_7 is sensitive between 500 and 2500 km and sets mainly the lower boundary of the gray envelope at those depths (Fig. 2c). As expected from the gravity harmonics equation, the odd harmonics, similarly to the even harmonics depth sensitivity, show that higher order harmonics are more sensitive in outer regions (Zharkov & Trubitsyn, 1974; Guillot & Gautier, 2007; Nettelmann et al., 2013). However, the depth dependence is more complicated when addressing the odd harmonics alone.

3.1.1 Contribution function

The depth sensitivity of the gravity harmonics can also be examined by calculating directly the depth dependence of J_n. Defined as the contribution function, that was calculated for the even harmonics of Jupiter and other planets (e.g. Guillot & Gautier, 2007; Helled et al., 2010; Nettelmann et al., 2013). The contribution of each shell is basically the normalized integrant of J_n, defined as $C_n = \frac{d\Delta J_n}{dr}/J_n$, where $\frac{d\Delta J_n}{dr} = -\frac{2\pi}{MR_J^n}\int_{-1}^{1}\rho\left(r,s\right)r^{n+2}P_n\left(\mu\right)d\mu$ (Zharkov & Trubitsyn, 1974; Hubbard et al., 1974; Hubbard, 1984). The even harmonics in these studies are calculated from the background density (solid body models), while in our study we use the wind-induced anomalous density field to calculate the odd harmonics contribution, so here $\rho = \rho'$. The odd contribution function of each odd gravity harmonic (Fig. 3b) is calculated from the average anomalous density profile (Fig. 3a) of all possible decay structures that are consistent with all Juno's four odd gravity har-

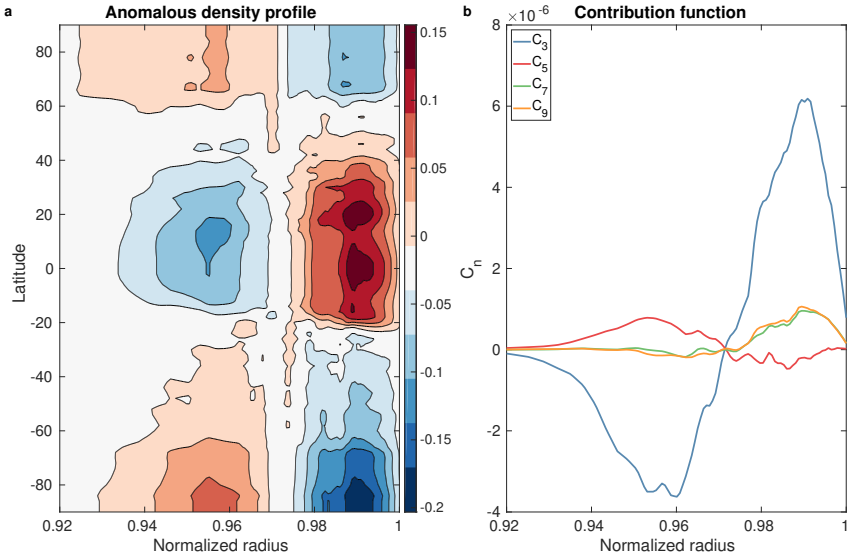

Figure 3. (a) The average anomalous density profile of all possible decay options that fits the Juno four measured odd gravity harmonics, colors represent anomalous density values range [kg m^{-3}] (b) the resulting contribution function for each of the odd gravity harmonics. Both panels are for all the latitudes and only for the upper $\sim$ 5000 km, below this depth the anomalous density equals zero.

monics allowed range (Fig. 1a). Note that here, unlike the even harmonics static contribution (e.g. Nettelmann et al., 2013), we do not have to normalize by the value of J_n since all four values are within the same order of magnitude, yet, we present the normalized result for convenient comparison.

The resulting contribution from the odd harmonics shows a very different pattern compared to the even harmonics discussed in Nettelmann et al. (2013). Most importantly, unlike the case of the even harmonics, the contribution here changes signs for all harmonics (Fig. 3b). The change of sign is consistent with depth in both panels. The integrals of the contribution curve are the gravity harmonic values, which for the averaged anomalous density are: $J_3\left(\times 10^{-8}\right) = -4.29$, $J_5\left(\times 10^{-8}\right) = -7.50$, $J_7\left(\times 10^{-8}\right) = 10.8$ and $J_9\left(\times 10^{-8}\right) = -6.69$. Interestingly, the contribution figure reveals a complex depth dependence for all four values. C_3, which has the largest contribution from each region, gets the biggest contribution from the upper part (the difference between the upper and lower parts constituted the J_3 value). C_5 is the only harmonic that most of its contribution raises from the deeper part of the density anomaly. This might explain the strong depth sensitivity of J_5 revealed in Fig. 3. C_7 and C_9 clearly depend much more on the upper part. The contribution function of the odd harmonics manifested in a more complicated pattern than the even harmonics. Unlike the even harmonics, which correspond only to the static shape of the planet, the higher odd harmonics are not simply more pronounced in the outer regions. The projection of the wind patterns onto different depths is reflected in the odd contribution in those depths, concealing the $(r/R_J)^n$ dependency which is the prominent feature for the even contribution.

3.2 Perturbed cloud-level wind profiles

Next we examine how perturbing the cloud-level wind (subsection 2.3) affects the ability to explain the odd gravity harmonics. The perturbed wind profiles (Fig. 4e, colors) result in a substantially bigger solutions envelope (Fig. 4a-d, gray) than the one from

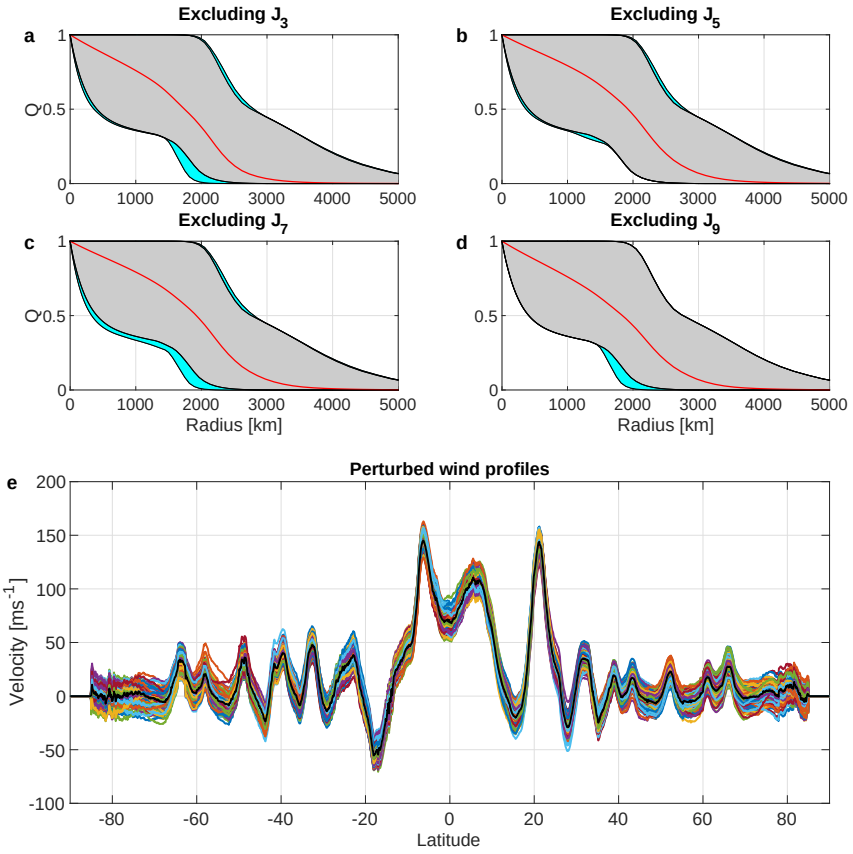

Figure 4. (a-d) Modified wind profiles odd gravity harmonics depth sensitivity summary as in Fig. 2 and (e) 100 examples of the 1000 profiles generated those odd harmonics values (colors) and Jupiter's measured wind profile (black). Each profile was examined with 5×10^5 random decay options. The results shown here are for all 5×10^8 options.

the measured zonal wind profile case, consistent with the fact that we allow a wider range of wind profiles. Note that the overall shape has changed and that the flow can even vanish at ~ 2500 km. This might have an important implication since the initial time dependent magnetic field results from Juno imply that the wind in those regions should be very weak (Duer et al., 2019; Moore et al., 2019). Also note that even for the perturbed winds there are no solutions fitting at least three odd J_n, that vanishes above 2000 km. The depth sensitivity of each harmonic is less unique than the measured wind case. This reflects the fact that Fig. 4 is a combination of all the possible solutions from 1000 examined meridional wind structures. Overall J_3 still seems to be the most sensitive harmonic in deeper regions, J_5 turns to be the most insignificant harmonic and J_9 does affect the depth range of $1500-2000$ km unlike the unperturbed wind case. The substantially larger area of solutions, however, does not manifested in more solutions relative to the examined cases. From 1000 examined profiles tested with 5×10^5 decay options each, only about 0.1% fit the anomalous gravity field compared to about 1% in the unperturbed case (Fig. 6, red and blue). This suggests that although other solutions exists for the cloud-level wind, it is likely that a structure that is similar to the observed cloud-level is indeed the structure in the deeper atmosphere of Jupiter.

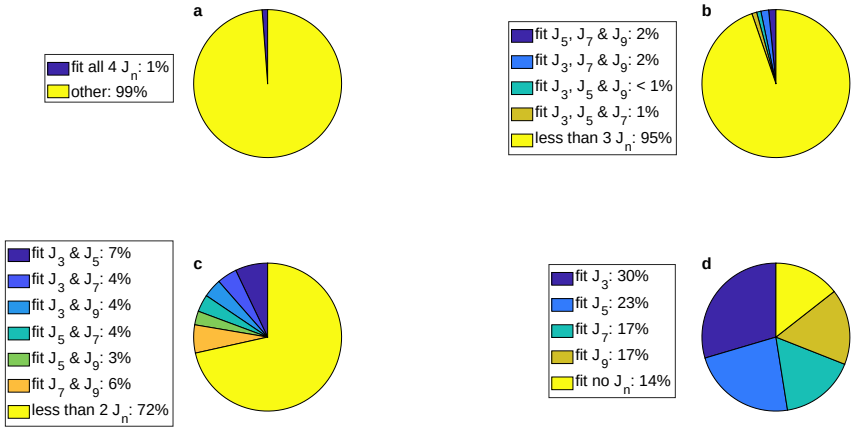

Figure 5. Summary of random meridional profiles correspondence to the odd gravity harmonics. Only $\sim$ 1% of the zonal profiles are able to fit all four odd gravity harmonics (a), 10% of the zonal profiles fit at least three odd gravity harmonics (b), 45% of the zonal profiles fit at least two odd gravity harmonics (c) and 6% fit non of the odd gravity harmonics (d). The full compatibility distribution is detailed in the figure.

3.3 Other cloud-level wind profiles

The resulting solution envelopes of the random wind profiles are relatively similar to the previous case of perturbed winds (not shown). However, the ability of the 1000 examined random profiles, each with 5×10^5 decay options, is considerably smaller than previous cases. Only about 0.01% fit all four odd gravity harmonics (Fig. 6, yellow). This clearly indicates that fitting all four odd numbers is very difficult with random meridional profiles of zonal wind. Moreover, Only a very small subset of profiles (13 examined meridional arrangements out of 1000, about 1%) are able to fit with any decay profile the measured four values (Fig. 5a), and in general, the measured numbers do not appear to be coincidental with the zonal flow structure. This should not come as a surprise since it is very unlikely that below the cloud level of Jupiter utterly different structure of zonal profile suddenly arise. Out of the 1000 profiles examined, combination of even two or more gravity harmonics is rare and exists in only 7% or less of the profiles (Fig. 5b,c).

A summary of all examined cases appears in Fig. 6. Note that the ordinate is a logarithmic scale and that 100% stands for all the zonal profiles (1000 zonal wind profiles other than the measured wind) and all decay options (5×10^5) for each case. We find that the envelope of possible solutions from Fig. 1 stands for only $\sim$ 1% of the tested vertical structures for zonal flows. The fitting percentage decreases with increasing perturbations, and drops rapidly when switching to random profiles. This trend repeats for all variations of only three odd harmonics. For all cases the random winds shows significantly lower fitting percentage than the other cases. We also present fitting percentage of excluding two and three harmonics (Fig. 1). This result strongly strengthens the assumption that Jupiter's meridional flow structure remains relatively unchanged beneath the cloud-level.

3.4 Depth dependent wind profile according to MWR measurements

The deconvolved nadir brightness temperature from Juno's microwave radiometer, as in Li et al. (2017), appear to be smoother with depth from channel six (cloud-level) towards channel one ($\sim$ 300 km depth) (Fig. 7, black lines). The most apparent feature of the Nadir temperature in channel one is that the equatorial anomaly remains, while

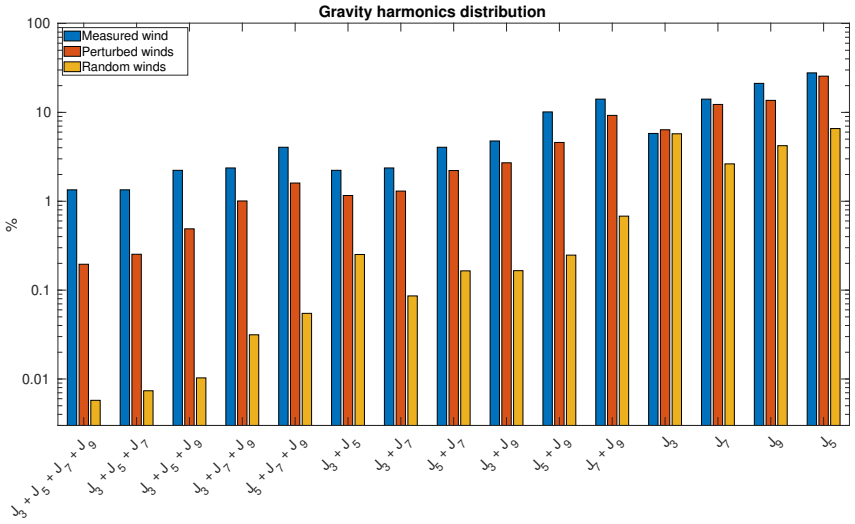

Figure 6. Solutions summary for the four presented cases of wind structures: Jupiter's measured wind at the cloud level (blue), 1000 slightly modified meridional structures (red) and 1000 random zonal profiles with similar general structure to Jupiter's zonal profile (yellow). The ordinate is a logarithmic scale of percentage relative to all cases that were examined. The particular requirement of the solution to match the different odd gravity harmonics is presented by the abscissa.

at higher latitudes the waviness dissolves. The relation between Jupiter's meridional profile and the brightness temperature is clear at the cloud-level (channel six) (Fig. 7a, top), yet it vanishes in the depths of the other channels, most prominently in channel one (Fig. 7a, bottom). The running average at depth allows to match between the temperature trend and the zonal jets. For comparison, three options for the deep winds are presented. The first, without depth dependence, is not consistent with the nadir temperature trend at depth (Fig. 7a). The other two panels, with increased relaxation with depth, are more compatible with the nadir temperature (Fig. 7b,c).

The examined cases cover the range of possibilities of altering the meridional profile with depth. The case studies range from slightly to largely modified depth dependent profile until no solutions are found (Fig. 8a). For slightly smoother profiles the ability to fit all four odd J_n is similar to that without any smoothing (Fig. 8a). Stronger smoothing leads to less ability to fit the odd four J_n. Using more than 10 degrees running average results in no solutions for the odd gravity harmonics. Comparison between the ability to fit the gravity harmonics while excluding one of them for the three case studied in Fig. 7 shows a steady tendency, with all the odd J_n affected by the relaxation until no solutions can be found (Fig. 8b).

4 Discussion and conclusions

The main challenge of interpreting the Juno gravity measurements is that the measurements provide only a handful of numbers (gravity harmonics), while the meridional and vertical profile of the interior flow have many degrees of freedom, and therefore by-definition the problem is ill-posed. Acknowledging this inherent issue, Kaspi et al. (2018) used four degrees of freedom for the vertical flow profile (matching the number of the four odd harmonics), and found the best optimized profile for this allowed range. They addressed the non-uniqueness by showing the statistical likelihood of wind profiles for

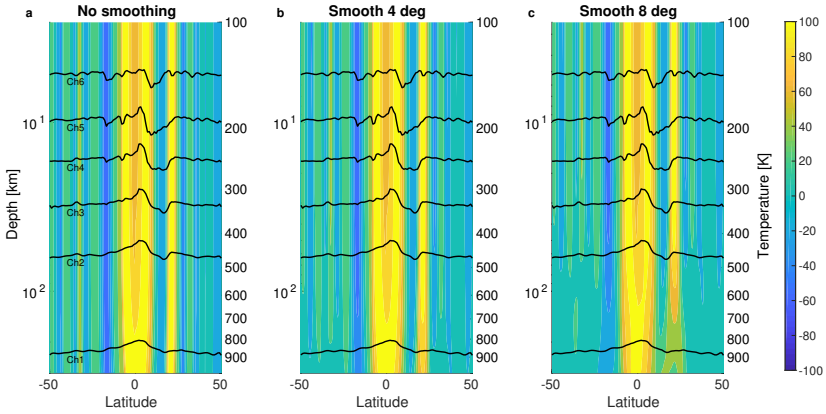

Figure 7. (a) Wind velocity (colors, [ms^{-1}]) between latitudes $-50°$ and $50°$ in the upper 300 km of Jupiter (left ordinate) combined with nadir brightness temperature lines from Juno's PJ1 (black, right ordinate), and two modified deep wind structures, (b) slightly modified with a running average of 4 degrees at 300 km and (c) a running average of 8 degrees at 300 km.

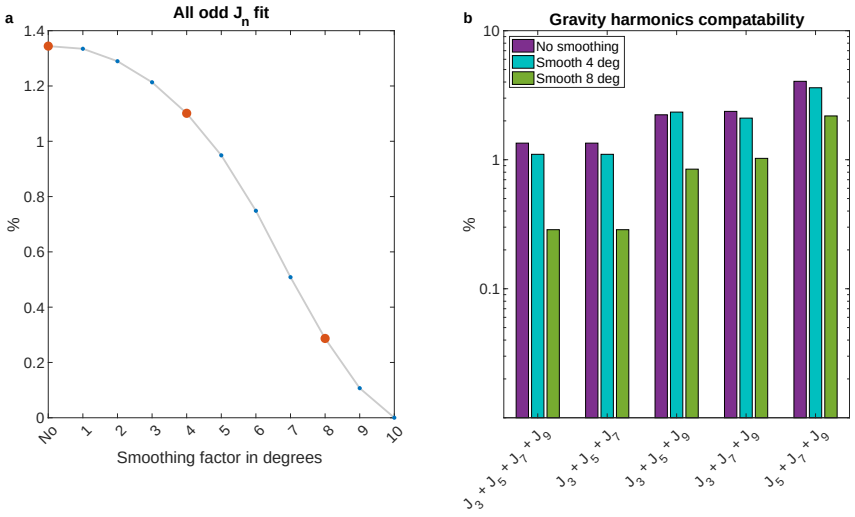

Figure 8. (a) The ability of the depth dependent wind profiles to fit all four odd gravity harmonics (percentage of solutions) as function of the smoothing factor in degrees (blue line). The three cases shown in Fig. 7 are denoted by red dots. (b) The gravity harmonics distribution for the red dots compatible to the three case studies in Fig. 7. The ordinate is a scale of percentage relative to the 5×10^5 random decay options examined.

the interior that are completely different than the cloud-level flow. Kong et al. (2018) highlighted the non-uniqueness issue by showing that two different flow profiles can still satisfy the gravity measurements. In this study we take a more methodological approach and consider a wider range of solutions and analyze their statistical likelihood. The flow profiles we consider, both for the meridional and vertical profiles, are bound by physical considerations. We also address two main issues: First, all previous studies looked at all four odd gravity harmonics together and found the flow profiles best matching all four. Here, we investigate how does each one of them separately bound the flow. Second, in attempt to coincide the gravity and microwave data, we explore if deep profiles that are smoother than those of the cloud-level, as possibility indicated by the microwave nadir temperature measurements, can be consistent with the gravity measurements.

Beginning with assuming that the cloud-level wind profile extends to depth with some decay profile, we identify the envelope of possible solutions (Fig. 1). We then relax the dependence on each of the odd gravity harmonics separately and by this analyze their individual contribution to the vertical profile of the zonal wind (Fig. 2). We find that J_3, which is the lowest order odd harmonic that represent the dynamics of Jupiter, is sensitive at depths where the conductivity rises (beyond $\sim$ 3000 km) and the magnetic field might be interacting with the flow, resulting in the Lorentz force playing a key role in the dynamics. J_5 appears to be the most sensitive harmonic, giving a robust constraint on the vertical structure of the zonal flow alone (Fig. 2b). Interestingly, J_9 does not give any new constraint on the flow if the other three harmonics are within the sensitivity range (Fig. 2d).

The modified zonal flows analysis revealed a substantially bigger possible solutions envelope than that with extending the cloud-level wind (Fig. 4). This implies that the depth sensitivity of each harmonic might alter with different structure of zonal wind, however the overall structure remains similar. Even for the perturbed winds, the flow cannot vanish shallower than 2000 km depth. The case with random winds implies that the wind cannot be completely altered below the cloud level, since fitting the four odd gravity harmonics (or three if we ignore J_9) is not coincidental and requires either similar winds to the measured ones that would penetrate few thousands of kilometers into the planet, or a very specific and statistically unlikely combination of meridional wind profile and a decay structure (Fig. 6). Finally, the gravity harmonics of the slightly modified depth dependent meridional profiles that are more compatible with the MWR measurements at depth are still within Juno's gravity measurements range, indicating that the nadir temperature could indeed reflect on the structure of the zonal jet at 300 km (channel 1) as it does at the cloud-level (Figs. 7,8).

Acknowledgments

We thank Cheng Li for providing the MWR data. This research has been supported by the Israeli Space Agency and the Helen Kimmel Center for Planetary Science at the Weizmann Institute of Science. Models used in this study are publicly available. The Juno gravity measurements (Iess et al., 2018) and MWR measurements (Li et al., 2017) are publicly available. Additional data can be found here
https://www.dropbox.com/sh/5fyg6a2aj6q9huc/AABuKUyWmuTKCZQg9k2Uak9Ta?dl=0.

References

Bolton, S. J., Adriani, A., Adumitroaie, V., Allison, M., Anderson, J., Atreya, S., ... Wilson, R. (2017). Jupiter's interior and deep atmosphere: The initial pole-to-pole passes with the Juno spacecraft. *Science*, *356*, 821-825.

Cao, H., & Stevenson, D. J. (2017). Zonal flow magnetic field interaction in the semi-conducting region of giant planets. *Icarus*, *296*, 59-72.

Duer, K., Galanti, E., & Kaspi, Y. (2019). Analysis of Jupiter's deep jets combin-

ing Juno gravity and time-varying magnetic field measurements. *Astrophys. J. Let.*, *879*(2), L22. doi: 10.3847/2041-8213/ab288e

French, M., Becker, A., Lorenzen, W., Nettelmann, N., Bethkenhagen, M., Wicht, J., & Redmer, R. (2012). Ab initio simulations for material properties along the Jupiter adiabat. *Astrophys. J. Sup.*, *202*, 5.

Galanti, E., Cao, H., & Kaspi, Y. (2017). Constraining Jupiter's internal flows using Juno magnetic and gravity measurements. *Geophys. Res. Lett.*, *44*, 8173-8181.

Galanti, E., Kaspi, Y., & Tziperman, E. (2017). A full, self-consistent, treatment of thermal wind balance on fluid planets. *J. Comp. Phys.*, *810*, 175-195.

Garcia-Melendo, E., P'erez-Hoyos, S., Sanchez-Lavega, A., & Hueso, R. (2011). Saturn's zonal wind profile in 2004–2009 from cassini iss images and its long-term variability. *Icarus*, *215*(1), 62-74.

Garcıa-Melendo, E., & Sánchez-Lavega, A. (2001). A study of the stability of jovian zonal winds from HST images: 1995–2000. *Icarus*, *152*(2), 316–330.

Gastine, T., Wicht, J., Duarte, L. D. V., Heimpel, M., & Becker, A. (2014). Explaining Jupiter's magnetic field and equatorial jet dynamics. *Geophys. Res. Lett.*, *41*, 5410-5419.

Guillot, T., & Gautier, D. (2007). Treatise of geophysics: 10. planets and moons. In T. Spohn & J. Schubert (Eds.), (pp. 439–464). Elsevier.

Guillot, T., Miguel, Y., Militzer, B., Hubbard, W. B., Kaspi, Y., Galanti, E., ... Bolton, S. J. (2018). A suppression of differential rotation in Jupiter's deep interior. *Nature*, *555*, 227-230.

Helled, R., Anderson, J. D., Podolak, M., & Schubert, G. (2010). Interior models of Uranus and Neptune. *Astrophys. J.*, *726*(1), 15.

Hubbard, W. B. (1984). *Planetary interiors.* pp. 343. New York, Van Nostrand Reinhold Co.

Hubbard, W. B. (2012). High-precision Maclaurin-based models of rotating liquid planets. *Astrophys. J. Let.*, *756*, L15.

Hubbard, W. B., Slattery, W. L., & Devito, C. L. (1975). High zonal harmonics of rapidly rotating planets. *Astrophys. J.*, *199*, 504-516.

Hubbard, W. B., Trubitsyn, V. P., & Zharkov, V. N. (1974). Significance of gravitational moments for interior structure of Jupiter and Saturn. *Icarus*, *21*(2), 147–151.

Iess, L., Folkner, W. M., Durante, D., Parisi, M., Kaspi, Y., Galanti, E., ... Bolton, S. J. (2018). Measurement of Jupiter's asymmetric gravity field. *Nature*, *555*(7695), 220-222.

Ingersoll, A. P., Adumitroaie, V., Allison, M. D., Atreya, S., Bellotti, A. A., Bolton, S. J., ... Steffes, P. G. (2017). Implications of the ammonia distribution on Jupiter from 1 to 100 bars as measured by the Juno microwave radiometer. *Geophys. Res. Lett.*, *44*(15), 7676–7685.

Jones, C. A., & Kuzanyan, K. M. (2009). Compressible convection in the deep atmospheres of giant planets. *Icarus*, *204*, 227-238.

Kaspi, Y. (2013). Inferring the depth of the zonal jets on Jupiter and Saturn from odd gravity harmonics. *Geophys. Res. Lett.*, *40*, 676-680.

Kaspi, Y., Davighi, J. E., Galanti, E., & Hubbard, W. B. (2016). The gravitational signature of internal flows in giant planets: comparing the thermal wind approach with barotropic potential-surface methods. *Icarus*, *276*, 170-181.

Kaspi, Y., Flierl, G. R., & Showman, A. P. (2009). The deep wind structure of the giant planets: Results from an anelastic general circulation model. *Icarus*, *202*, 525-542.

Kaspi, Y., Galanti, E., Hubbard, W. B., Stevenson, D. J., Bolton, S. J., Iess, L., ... Wahl, S. M. (2018). Jupiter's atmospheric jet-streams extend thousands of kilometers deep. *Nature*, *555*, 223-226.

Kaspi, Y., Hubbard, W. B., Showman, A. P., & Flierl, G. R. (2010). Gravitational signature of Jupiter's internal dynamics. *Geophys. Res. Lett.*, *37*, L01204.

Kong, D., Zhang, K., Schubert, G., & Anderson, J. D. (2018). Origin of Jupiter's cloud-level zonal winds remains a puzzle even after Juno. *Proc. Natl. Acad. Sci. U.S.A.*, *115*(34), 8499–8504. doi: 10.1073/pnas.1805927115

Li, C., Ingersoll, A., Janssen, M., Levin, S., Bolton, S., Adumitroaie, V., ... Williamson, R. (2017). The distribution of ammonia on Jupiter from a preliminary inversion of Juno microwave radiometer data. *Geophys. Res. Lett.*, *44*(11), 5317–5325.

Liu, J., Goldreich, P. M., & Stevenson, D. J. (2008). Constraints on deep-seated zonal winds inside Jupiter and Saturn. *Icarus*, *196*, 653-664.

Moore, K. M., Cao, H., Bloxham, J., Stevenson, D. J., Connerney, J. E., & Bolton, S. J. (2019). Time-variation of Jupiter's internal magnetic field consistent with zonal wind advection. *Nature Astronomy*, 1.

Nellis, W. J., Mitchell, A. C., McCandless, P. C., Erskine, D. J., & Weir, S. T. (1992). Electronic energy gap of molecular hydrogen from electrical conductivity measurements at high shock pressures. *Phys. Rev. Let.*, *68*(19), 2937.

Nettelmann, N., Helled, R., Fortney, J. J., & Redmer, R. (2013). New indication for a dichotomy in the interior structure of Uranus and Neptune from the application of modified shape and rotation data. *Planatary and Space Science*.

Nettelmann, N., Püstow, R., & Redmer, R. (2013). Saturn layered structure and homogeneous evolution models with different eoss. *Icarus*, *225*(1), 548–557.

Pedlosky, J. (1987). *Geophysical fluid dynamics.* pp. 710. Springer-Verlag.

Salyk, C., Ingersoll, A. P., Lorre, J., Vasavada, A., & Del Genio, A. D. (2006). Interaction between eddies and mean flow in Jupiter's atmosphere: Analysis of Cassini imaging data. *Icarus*, *185*, 430-442.

Showman, A. P., & Kaspi, Y. (2013). Atmospheric dynamics of brown dwarfs and directly imaged giant planets. *Astrophys. J.*, *776*, 85-103.

Tollefson, J., Wong, M. H., de Pater, I., Simon, A. A., Orton, G. S., Rogers, J. H., ... S., M. P. (2017). Changes in Jupiter's zonal wind profile preceding and during the Juno mission. *Icarus*, *296*, 163-178.

Weir, S. T., Mitchell, A. C., & Nellis, W. J. (1996). Metallization of fluid molecular hydrogen at 140 GPa (1.4 mbar). *Phys. Rev. Let.*, *76*, 1860-1863.

Zharkov, V. N., & Trubitsyn, V. P. (1974). Determination of the equation of state of the molecular envelopes of Jupiter and Saturn from their gravitational moments. *Icarus*, *21*(2), 152–156.